Robotica (1999) volume 17, pp. 173–179. Printed in the United Kingdom © 1999 Cambridge University Press

An improved pseudoinverse solution for redundant hydraulic manipulators

L. Beiner* and J. Mattila†

(Received in Final Form: September 6, 1998)

SUMMARY

The paper deals with the kinematic redundancy control of a 3DOF linear hydraulic manipulator moving in the vertical plane. The analysis is carried out in actuator coordinates so as to make the results usable in control schemes with actuator position feedback. The idea is to use the initial manipulator configuration as an optimization parameter in order to: (I) further minimize the actuator velocities obtained by a pseudoinverse solution, (II) simultaneously avoid actuator limits without recourse to a gradient projection approach. An improved pseudoinverse redundancy solution is thus obtained and implemented in a simple, non-iterative algorithm suitable for real-time applications. Simulations of a typical task with the proposed method show that minimizing the actuator velocity norm yields better results than minimizing the manipulator kinetic energy.

KEYWORDS: Pseudoinverse solution; Hydraulic manipulators; Redundancy control; Real-time applications.

1. INTRODUCTION

Redundancy resolution of robotic mechanisms by local or global optimization has been extensively discussed in the literature. Most methods for solving redundancy by local optimization use the pseudoinverse-based solution introduced in reference 1 and extended by a gradient projection method in reference 2 illustrated below

$$\dot{\theta}=J^{+}\dot{y}+(I-J^{+}J)z \tag{1}$$

where y is the m-vector of Cartesian coordinates of the end-effector, θ denotes the n-vector of joint variables, $(n>m)$, J^{+} denotes the Moore-Penrose pseudoinverse of the Jacobian matrix, J, $(I-J^{+}J)$ is the null-space projection matrix and z is an arbitrary vector in the null-space of the Jacobian. The first term of Eq. (1) is the pseudoinverse solution fulfilling the primary goal of following a given trajectory, while in the second term the null-space vector can be set to correspond to the gradient of various optimization functions $\Phi(\theta)$, i.e., $z=\alpha\nabla\Phi(\theta)$. It is thus possible to specify a number of secondary optimization objectives, such as joint limit avoidance,[2,3] obstacle avoidance,[4,5] joint torque minimization,[6] joint acceleration optimization,[7] and maximization of various end-effector dexterity measures.[8,9] All these solutions are local, in the sense that they deal with the instantaneous kinematics of motion, i.e., motion that is locally optimized by incremental movement from the current manipulator state. Motivation for the present study has been provided by the fact that the influence of the initial robot configuration on the redundancy solution has not yet been considered. In this context, the contributions of the present study dealing with the redundancy resolution of a 3DOF hydraulic manipulator are as follows. First, the initial configuration is used in a non-iterative optimization algorithm that improves the pseudoinverse solution and simultaneously avoids the actuator limits. Second, the solution is developed in actuator coordinates, thus making it usable in computed-force control algorithms with actuator position feedback.[10,11] The approach is illustrated by simulating a typical task using two improved pseudoinverse solutions, one minimizing the norm of actuator velocities and the other the kinetic energy.

* Center for Technological Education Holon (affiliated with Tel Aviv University), P.O. Box 305, IL-58102, Holon (Israel)
† Institute of Hydraulics and Automation, Tampere University of Technology, P.O. Box 589, FIN-33301, Tampere (Finland).

2. ANALYSIS

Consider the common type of serial hydraulic manipulator driven by linear actuators shown in Figures 1a and 1b and moving in the vertical plane. Here W denotes the load, W_1, W_2 and L_1, L_2 – the weight of booms 1 and 2 and their lengths, respectively, W_3 and L_3 – the weight and length of the telescope, θ_1, θ_2 – the manipulator angles (positive counterclockwise), e, c, L_{11}, L_{12}, L_{21}, L_{22}, α_1, α_2, β_1, β_2 – specified lengths and angles, and x_1, x_2, x_3–the actuator lengths, where $L_2+x_3=L_3+d_3$. From Figs. 1a and 1b the relationships between the manipulator angles θ_1, θ_2 and the joint coordinates q_1, q_2 are obtained as follows

$$\theta_1=q_1+c_1,\ c_1=-\pi/2+(\alpha_1+\alpha_2) \tag{2}$$

$$\theta_2=q_2+c_2,\ c_2=\beta_1+\beta_2-\pi \tag{3}$$

In the y_1-y_2 coordinate system of Figure 1, the joint-to-Cartesian transformation is expressed by

$$\begin{aligned} y_1&=L_1\cos\theta_1+(L_3+d_3)\cos(\theta_1+\theta_2)-e\\ &=L_1\cos(q_1+c_1)+(L_3+d_3)\cos(q_1+q_2+c_1+c_2)-e \end{aligned} \tag{4}$$

$$\begin{aligned} y_2&=L_1\sin\theta_1+(L_3+d_3)\sin(\theta_1+\theta_2)+c\\ &=L_1\sin(q_1+c_1)+(L_3+d_3)\sin(q_1+q_2+c_1+c_2)+c \end{aligned} \tag{5}$$

which can be written in a more compact form and differentiated twice to give

$$y=h_1(q) \tag{6}$$

$$\dot{y}=\frac{\partial h_1}{\partial q}\dot{q}=J(q)\dot{q} \tag{7}$$

https://doi.org/10.1017/S0263574799001216 Published online by Cambridge University Press

$$\ddot{y} = J(q)\ddot{q} + \dot{J}(q)\dot{q} \tag{8}$$

where J denotes the Jacobian of the joint-to-Cartesian transformation (6). The joint-to-actuator transformation is obtained from Figure 1 as

$$x_i = \sqrt{L_{i1}^2 + L_{i2}^2 - 2L_{i1}L_{i2}\cos q_i},\ i = 1,2,\ x_3 = d_3 - L_2 + L_3 \tag{9}$$

which can also be rewritten in a more compact form and differentiated twice to give

$$x = h_2(q) \tag{10}$$

$$\dot{x} = \frac{\partial h_2}{\partial q}\dot{q} = A(q)\dot{q} \tag{11}$$

$$\ddot{x} = A(q)\ddot{q} + \dot{A}(q)\dot{q} \tag{12}$$

where the Jacobian A takes the form

$$A = \begin{bmatrix} a_1 & 0 & 0 \\ 0 & a_2 & 0 \\ 0 & 0 & 1 \end{bmatrix} \tag{13}$$

a_i, $i = 1,2$ being the torque arms of actuator forces F_1 and F_2 given by

$$a_i = L_{1i}L_{2i}\sin q_i / x_i \tag{14}$$

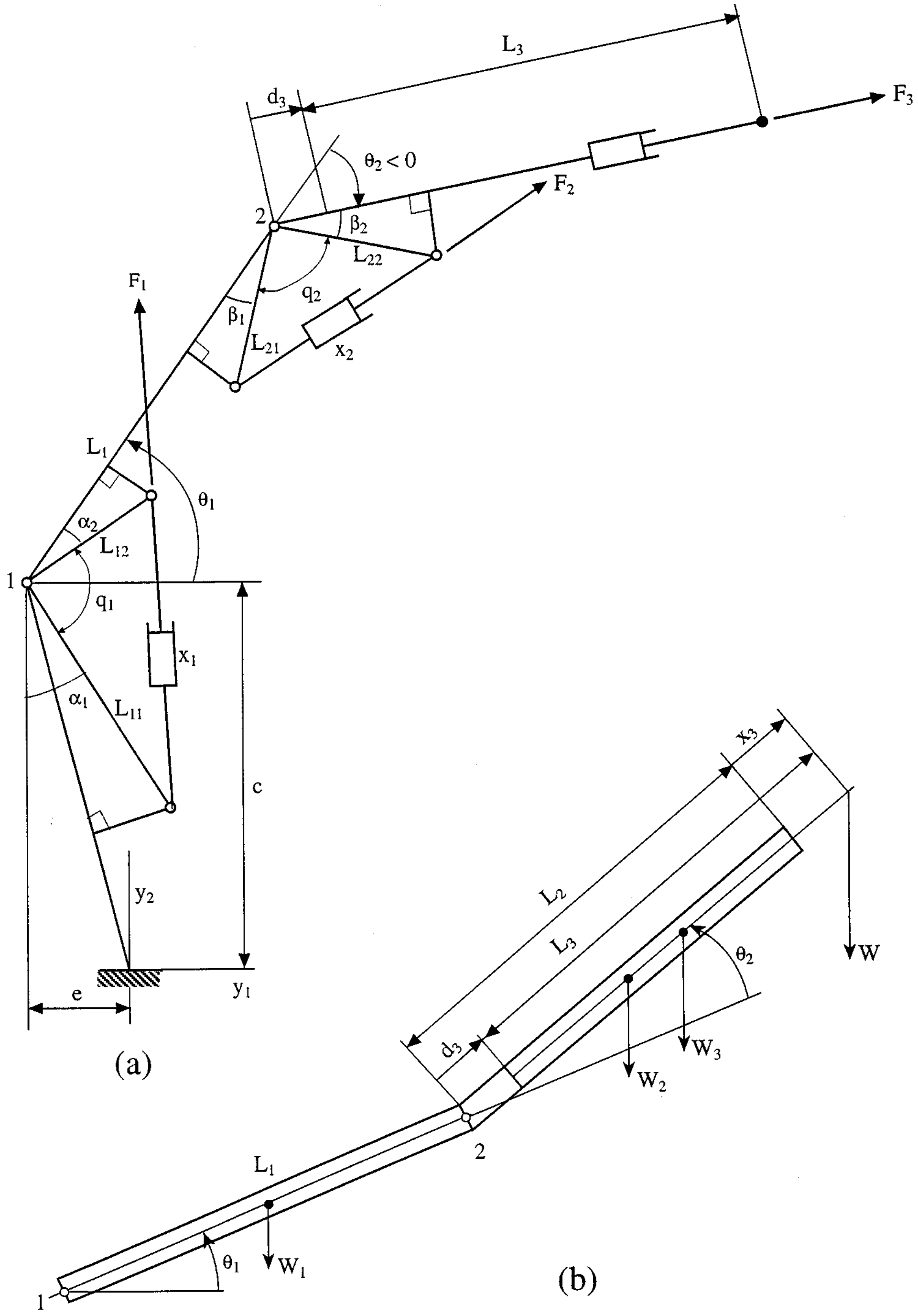

Fig. 1. 3-DOF hydraulic manipulator in the vertical plane.

https://doi.org/10.1017/S0263574799001216 Published online by Cambridge University Press

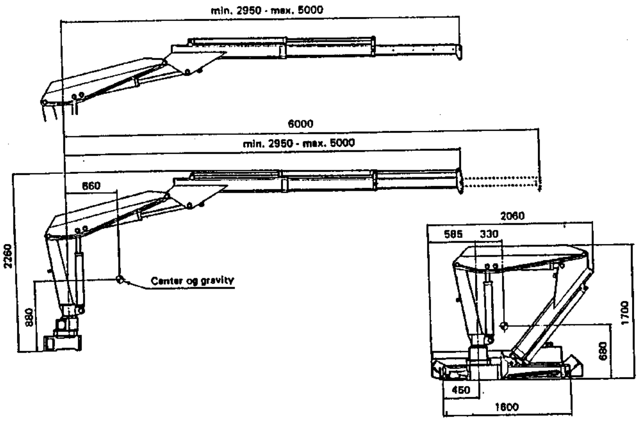

Fig. 2. HIAB 031 hydraulic crane.

The diagonal matrix A thus gives the relationship between joint torques τ and actuator forces F as ($A^T = A$)

$$\tau = AF$$

Combining Equations (7)–(8) and (11)–(12) yields the following actuator-to-Cartesian kinematic relationships between velocities and accelerations

$$\dot{y} = JA^{-1}\dot{x} \tag{16}$$

$$\ddot{y} = JA^{-1}\ddot{x} + (\dot{J} - JA^{-1}\dot{A})A^{-1}\dot{x} \tag{17}$$

A novel approach used in this study consists in developing the manipulator kinematics and dynamics in actuator coordinates rather than in the usual joint space coordinates.[10,11] This was done with a view toward the real-time implementation of model-based computed-force control laws, since actuator coordinates can easily be measured and used for position feedback. Neglecting joint friction and disturbance terms, the equations of motion of a serial n-joint manipulator can be written in joint coordinates q as

$$M(q)\ddot{q} + V(q,\dot{q}) + G(q) = \tau \tag{18}$$

where $M(q)$ is the inertia matrix, $V(q,\dot{q})$ is the matrix of centrifugal and Coriolis terms, and $G(q)$ is the gravitation torque vector. Solving Equation (12) for $\ddot{q}$ and replacing $\dot{q}$ from Equation (11) gives

$$\ddot{q} = A^{-1}(\ddot{x} - \dot{A}\dot{q}) = A^{-1}(\ddot{x} - \dot{A}A^{-1}\dot{x}) \tag{19}$$

Replacing τ and $\ddot{q}$ from Equations (15) and (19), respectively, in Equation (18) and solving for the actuator forces, the manipulator equations of motion in terms of the actuator linear coordinates x and forces F are obtained as

$$F = A^{-1}MA^{-1}\ddot{x} - A^{-1}MA^{-1}\dot{A}A^{-1}\dot{x} + A^{-1}N \tag{20}$$

where the vector term $N(q,\dot{q}) = V(q,\dot{q}) + G(q)$ includes the nonlinear terms. Equation (20) can be rewritten in a more compact form as

$$F_H = M_H\ddot{x} + N_H \tag{21}$$

where

$$M_H = A^{-1}MA^{-1} \tag{22}$$

$$N_H = A^{-1}N - M_h\dot{A}A^{-1}\dot{x}, \tag{23}$$

and the subscript H indicates hydraulic actuator coordinates.

Specializing Equation (1) to actuator coordinates, the *unweighted* pseudoinverse redundancy solution yielding the actuator velocities required to follow a desired trajectory $y_d(t)$ is obtained from Equation (16) as

$$\dot{x} = J_H^{+}\dot{y}_d \tag{24}$$

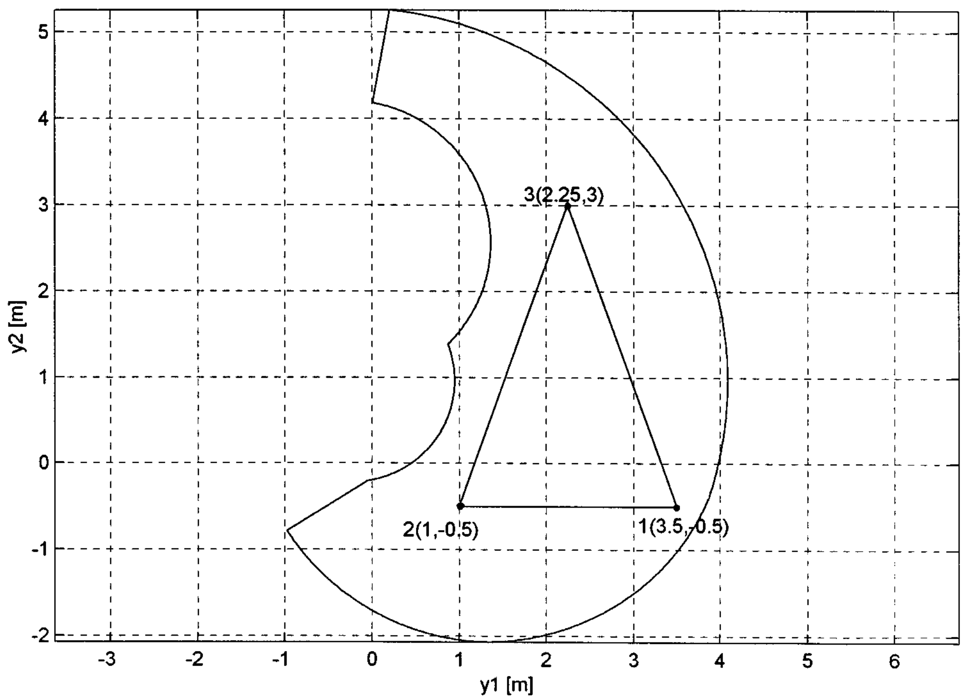

Fig. 3. HIAB 031 workspace and test task.

https://doi.org/10.1017/S0263574799001216 Published online by Cambridge University Press

where

$$J_H = JA^{-1} = J\begin{bmatrix} 1/a_1 & 0 & 0 \\ 0 & 1/a_2 & 0 \\ 0 & 0 & 1 \end{bmatrix} \qquad (25)$$

$$J_H^+ = J_H^T(J_H J_H^T)^{-1} \qquad (26)$$

which results in a *minimum velocity norm* solution (min $\dot{x}^T\dot{x}$). Since in this way the sum of squares of actuator velocities is minimized, the kinetic energy is also approximately minimized. A different way to realize desired performance characteristics is the *weighted* pseudoinverse. The pseudoinverse that minimizes the cost $\dot{x}^TWx$ is

$$J_W^+ = W^{-1}J^T(JW^{-1}J^T)^{-1} \qquad (27)$$

where W is an appropriately chosen weighting matrix. For a true minimization of the kinetic energy, the pseudoinverse must be weighted with the manipulator inertia matrix M_H. The kinetic energy is

$$T_H = \frac{1}{2}\dot{x}^T M_H \dot{x} \qquad (28)$$

and the weighted pseudoinverse that instantaneously minimizes $\dot{x}^TM_H\dot{x}$ is given by Equation (27) with $W=M_H$

$$J_{MH}^+ = M_H^{-1}J_H^T(J_H M_H^{-1}J_H^T)^{-1} \qquad (29)$$

where the mass matrix in actuator coordinates is given by

$$M_H = A^{-1}MA^{-1} = \begin{bmatrix} m_{11}/a_1^2 & m_{12}/a_1a_2 & m_{13}/a_1 \\ m_{21}/a_1a_2 & m_{22}/a_2^2 & m_{23}/a_2 \\ m_{31}/a_1 & m_{32}/a_2 & m_{33} \end{bmatrix} \qquad (30)$$

$$m_{11} = 2L_1M\cos\theta_2(d_3+L_3) + M[(d_3+L_3)^2+L_1^2] + \frac{1}{3}\rho_1L_1^3$$

$$+\frac{1}{3}(L_2^3\rho_2+L_3^3\rho_3) + L_1\cos{}_2(\rho_2L_2^2+\rho_3L_3^2) + L_1^2(L_2\rho_2+L_3\rho_3)$$

$$+2L_3\rho_3L_1d_3\cos\theta_2 + L_3\rho_3d_3^2 + L_3^2\rho_3d_3$$

$$m_{12} = m_{21} = M(L_1d_3\cos\theta_2 + (d_3+L_3)^2 + L_1L_3\ \cos\theta_2$$

$$+\frac{1}{3}(L_2^3\rho_2+L_3^3\rho_3)\ \frac{1}{2}L_1\cos\theta_2(L_2^2\rho_2+L_3^2\rho_3) \qquad (31)$$

$$+L_3\rho_3L_1d_3\cos\theta_2 + L_3\rho_3d_3^2 + L_3^2\rho_3d_3$$

$$m_{13} = m_{31} = (L_1L_3\rho_3 + L_1M)\sin\theta_2$$

$$m_{22} = \frac{1}{3}(\rho_2L_2^3+\rho_3L_3^3) + L_3\rho_3d_3^2 + L_3^2\rho_3d_3 + M(d_3+L_3)^2$$

$$m_{23} = m_{32} = 0$$

$$m_{33} = L_3\rho_3 + M$$

Thus, the weighted pseudoinverse solution is

$$\dot{x} = J_{MH}^+\dot{y}_d \qquad (32)$$

which is a *minimum kinetic energy* solution (min $\dot{x}^T M_H\dot{x}$).

An improved pseudoinverse solution is proposed now which further reduces the peak min $\dot{x}^T\dot{x}$ or min$\dot{x}^TM_H\dot{x}$ values and simultaneously avoids the actuator bounds. The idea is to use to this end the initial manipulator configuration as an optimization parameter and the algorithm proceeds as follows:

(i) Define the desired trajectory $y_d(t)$.

(ii) Choose the initial telescope extension x_{3init} as an optimization parameter defining the initial manipulator configuration (the initial extensions x_{1init} or x_{2init} of actuators 1 or 2, respectively, can be chosen as well).

(iii) Start a loop sampling x_{3init} values in the specified admissible range $[x_{3min}, x_{3max}]$.

(iv) For each x_{3init} value, find by inverse kinematics the initial manipulator configuration and compute the time-histories of actuator velocities, displacements and actuator velocity norm or kinetic energy along the desired trajectory from $t=0$ to $t=t_f$ using either Equation (24) or (32). Then:
   - If $x_1 \in [x_{1\min}, x_{1\max}]$&$x_2 \in [x_{2\min}, x_{2\max}]$ along the entire trajectory, find the maximum value of the velocity norm or kinetic energy and save it together with the corresponding x_{3init} value. Then, go to the next x_{3init} value.
   - Else, go to the next x_{3init} value.

(v) When the x_{3init} loop is finished, the optimal x_{3init} value is the one corresponding to the lowest velocity norm or kinetic energy, which automatically also satisfies the actuator displacement constraints along the whole path.

As it appears, the above algorithm is both simple (it involves only a search of the pseudoinverse redundancy solution along the specified path) and fast (it is noniterative, in contrast to the gradient projection approach), being therefore most suitable for real-time control.

3. EXAMPLE

The proposed solution was tested through simulations performed with the HIAB 031 hydraulic crane shown in Figure 2. The crane parameters and joint limits (see notation in Figure 1) are given below:

$L_1=1.600$ m; $L_2=1.650$ m; $L_3=1.470$ m; $L_{11}=1.037$ m; $L_{12}=0.376$ m; $L_{21}=1.130$ m; $L_{22}=0.310$ m; $e=0.228$ m; $c=0.957$ m; $\alpha_1=21.7°$; $\alpha_2=10.6°$; $\beta_1=27.1°$; $\beta_2=2.93°$; $\rho_1=80/$ L_1 kg/m; $\rho_2=100/L_2$ kg/m; $\rho_3=36/L_3$ kg/m; $x_1\in[0.830,1.375]$m; $x_2\in[0.830,1.375]$m; $x_3\in[0,1.090]$m; $d_3=0.180\div1.270$ m; $\theta_{1\min}=-10.3°$; $\theta_{1\max}=92.1°$; $\theta_{2\min}=-137.6°$; $\theta_{2\max}=-12.4°$.

Using the specified joint limits in conjunction with the direct kinematics Equations (4)–(5), the crane workspace takes the shape shown in Figure 3. On the same figure is

https://doi.org/10.1017/S0263574799001216 Published online by Cambridge University Press

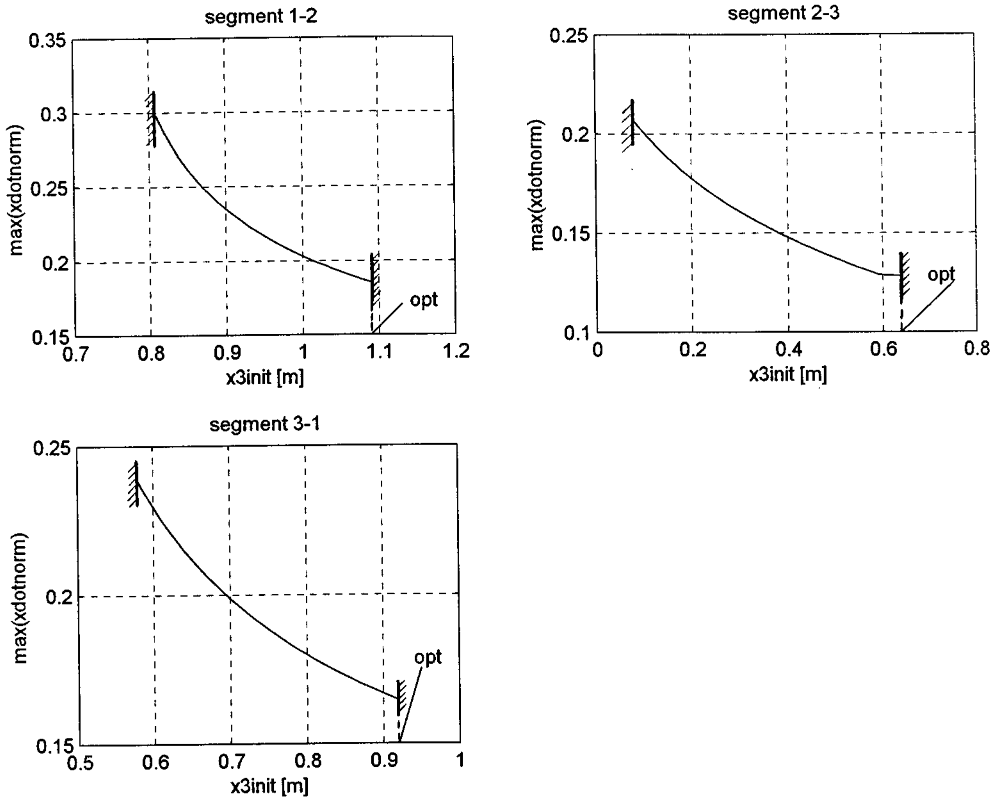

Fig. 4a. Variation of peak $\dot{x}^T\dot{x}$ with the initial telescope extension.

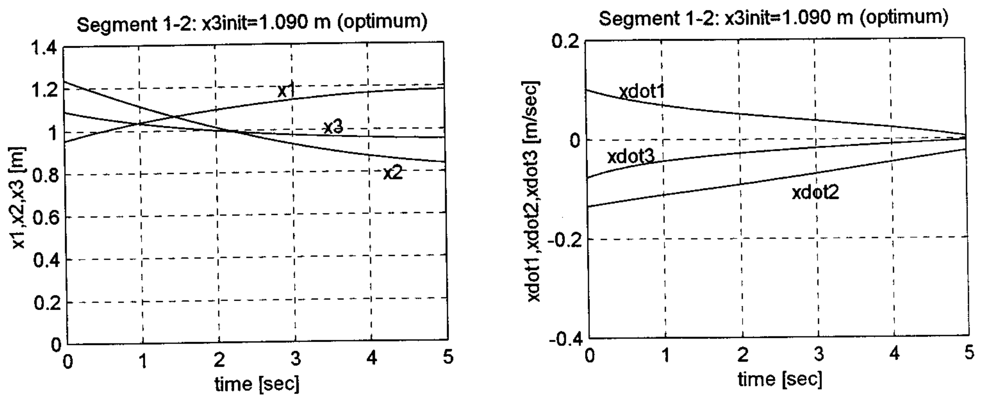

Fig. 4b. Min($\dot{x}^T\dot{x}$) actuator displacements and velocities along segment 1-2.

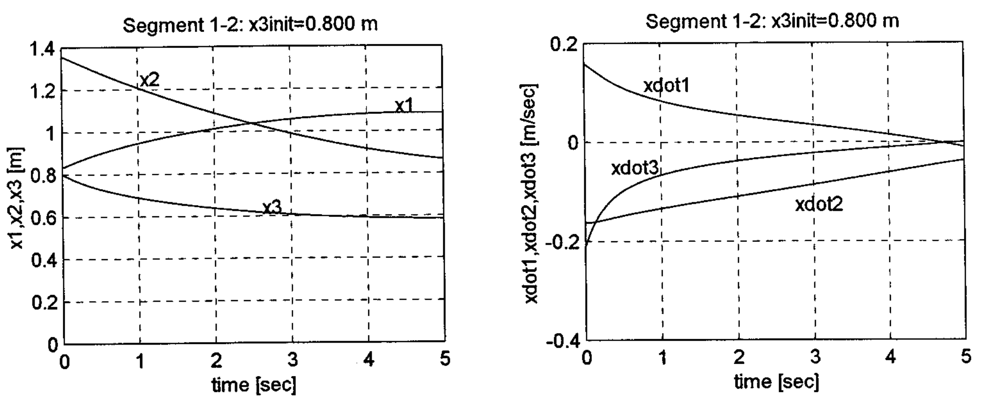

Fig. 4c. Nonoptimal actuator displacements and velocities along segment 1-2.

https://doi.org/10.1017/S0263574799001216 Published online by Cambridge University Press

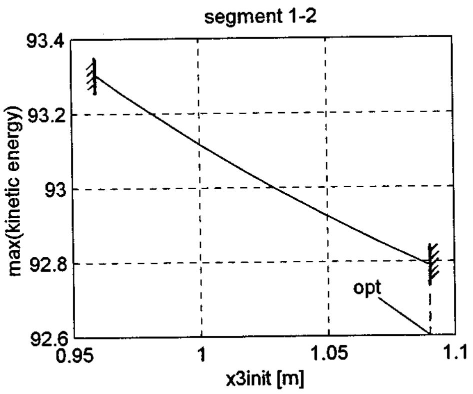

Fig. 5a. Variation of peak $\dot{x}^T M_H \dot{x}$ with the initial telescope extension.

displayed a typical task consisting of three linear segments connecting points 1 (3.5,-0.5), 2 (1,-0.5) and 3 (2.25,3). The work cycle is as follows: 1-2 (horizontal scraping action), 2-3 (extension to a dumping position), and 3-1 (return to the starting position). For ease of comparison, it is assumed that the end-effector tracks all segments with a constant velocity of 0.5 m/sec. Accordingly, the parametric equations of a linear trajectory P–Q traveled uniformly in a time t_f are

$$y_d = \begin{bmatrix} y_{1d} \\ y_{2d} \end{bmatrix} = \begin{bmatrix} y_{1Q} + (1 - t/t_f)(y_{1P} - y_{1Q}) \\ y_{2Q} + (1 - t/t_f)(y_{2P} - y_{2Q}) \end{bmatrix} \tag{33}$$

yielding by differentiation

$$\dot{y}_d = \begin{bmatrix} \dot{y}_{1d} \\ \dot{y}_{2d} \end{bmatrix} = \begin{bmatrix} -(y_{1P} - y_{1Q})/t_f \\ -(y_{2P} - y_{2Q})/t_f \end{bmatrix} \tag{34}$$

Simulations of the motion along the test task have been performed using the improved $\min \dot{x}^T \dot{x}$ and $\min \dot{x}^T M_H \dot{x}$ solutions. The results are presented in Figs. 4 and 5, respectively.

- Improved $\min \dot{x}^T \dot{x}$ solution: Figure 4a reveals the main finding, namely that the peak actuator velocity norm clearly depends on the initial manipulator configuration, decreasing substantially with the initial telescope extension x_{3init} along all task segments. Accordingly, the best initial configuration for minimizing actuator velocities is always with the telescope extended as much as feasible for a specific task segment. The ranges of feasible x_{3init} values indicated for each segment ensure that none of the actuator limits is exceeded. Reduction of the peak velocity norm results in lower and smoother actuator velocities and displacements, as shown by comparing an optimal solution (Figure 4b) with a non-optimal one (Figure 4c).
- Improved $\min \dot{x}^T M_H \dot{x}$ solution: Figure 5a shows that only a marginal reduction of the peak kinetic energy norm and a narrow feasible x_{3init} range are obtained in this case. Furthermore, the algorithm tends to minimize the kinetic energy by using the actuator x_1 the least and the telescope x_3 the most, which results in higher and steeper telescope velocities and displacements (Figure 5b).

4. CONCLUSION

An improved pseudoinverse solution for a 3DOF redundant crane with linear hydraulic actuators has been presented. The analysis has been performed in the actuator space so as to make the results applicable in control schemes with actuator position feedback. It is shown that by using the initial manipulator configuration as an optimization parameter, it is possible to reduce the actuator velocities obtained by a pseudoinverse solution and simultaneously avoid the actuator limits. The solution is implemented in a simple and noniterative algorithm. Simulations of a typical task show that the best initial configuration is with the telescope extended as much as feasible. A comparison between the improved min(actuator velocity norm) and min(kinetic energy) solutions indicates that the former results in lower and smoother actuator velocities and displacements than the latter.

References

1. D.E. Whitney, “Resolved motion rate control of manipulators and human prostheses” *IEEE Trans. on Man-Mach. Sys.*, **10**, No. 2, 47–53 (1969).
2. A. Liegeois, “Automatic supervisory control of the configuration and behavior of multibody mechanisms” *IEEE Trans. Sys., Man, Cybern.* **7**, No. 12, 868–871 (1977).

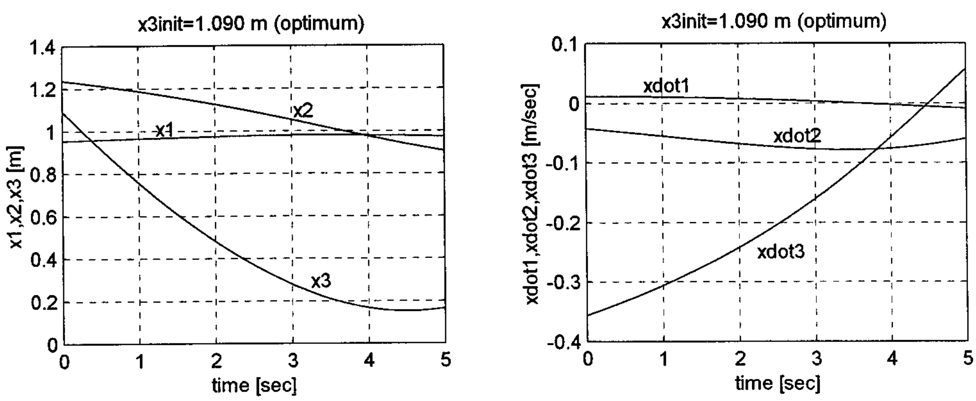

Fig. 5b. Min($\dot{x}^T M_H \dot{x}$ actuator displacements and velocities along segment 1-2.

https://doi.org/10.1017/S0263574799001216 Published online by Cambridge University Press

3. N. Singh, H. Zghal, N. Sepehri, S. Balakrishnan and P.D. Lawrence, "Coordinated-motion control of heavy-duty industrial machines with redundancy" *Robotica*, **13** Part 6, 623–633 (1995).
4. M. Kircanski and M. Vukobratovic, "Trajectory planning of redundant manipulators in the presence of obstacles" *Proc. 5th CISM-IFToMM Symposium Theory and Practice of Robots and Manipulators*, Udine, Italy, (1984) pp. 43–50.
5. A. Macijewski and C. Klein, "Obstacle avoidance for kinematically redundant manipulators in dynamically varying environments" *Int. J. Robotics Res.* **4**, 109–117 (1987).
6. J.M. Hollerbach and K.C. Suh, "Redundancy resolution of manipulators through torque optimization" *IEEE J. Robotics and Automat.* **3**, No. 4, 308–316 (1987).
7. A.A. Mohamed and C. Chevallereau, "Resolution of robot redundancy in the Cartesian space by criteria optimization" *Proc. IEEE Int. Conf. Robotics and Automat.* (1993) pp. 646–651.
8. T. Yoshikawa, "Analysis and control of robot manipulators with redundancy" **In:** *Robotics Research: The First International Symposium* (M. Brady and R. Paul, Eds.), (MIT Press, Cambridge, MA, 1984) pp. 735–748.
9. C.A. Klein and B.E. Blaho, "Dexterity measures for the design and control of kinematically redundant manipulators" *Int. J. Robotic Res.* **6**, 72–83 (1987).
10. J. Mattila and T. Virvalo, "Computed force control of hydraulic manipulators" *Proc. 5th Scandinavian Int. Conf. on Fluid Power*, Linkoeping, Sweden (1997) pp. 139–154.
11. J. Mattila and T. Virvalo, "On the energy efficient motion control of a 3 DOF hydraulic crane with computed force control method" *Proc. First Int. Fluid Power Conf.*, Aachen, Germany (1998) pp. 375–388.